

## Optical characterization of a-C:H thin films

J. González-Hernández

*Departamento de Física, Centro de Investigación y de Estudios Avanzados,  
Instituto Politécnico Nacional, apartado postal 14-740, México, D.F.*

R. Asomoza

*Departamento de Ingeniería Eléctrica, Centro de Investigación y de Estudios Avanzados,  
Instituto Politécnico Nacional, apartado postal 14-740, México, D.F.*

A. Reyes-Mena

*Centro de Investigación y de Estudios Avanzados-Mérida, Instituto Politécnico Nacional,  
Mérida, Yucatán*

(recibido el 10 de septiembre de 1987; aceptado el 19 de noviembre de 1987)

**Abstract.** We prepared amorphous hydrogenated carbon films from several different hydrocarbons as starting gases in a stainless steel UHV chamber, using a RF-excitation source at different powers. We analyzed the Vicker's hardness and the optical properties of the films using optical absorption, photoluminescence, Raman, and infrared spectroscopy. The changes in the structure due to different RF-power densities during deposition are closely related to their optical properties. Raman measurements provide clear evidence of graphitic-like regions, whereas photoluminescence indicates the presence of atoms having the four fold coordination. The volume fraction of graphitic-like phase increases with higher RF-power densities.

**PACS:** 78.20.Bh

### 1. Introduction

Research activity on amorphous semiconductors has been quite extensive for several years [1]. The ability to control the optical and electrical properties is important in the drive to replace crystalline and polycrystalline materials with amorphous thin films. While recent discoveries with device potential have been made, the main interest in the subject remains in the realm of basic physics. Some of the fundamental questions, to which only incomplete answers exist, concern the band structure of solids lacking long-range order, how current is conducted in such solids, how excess carriers recombine in them, and how structure and electronic properties are related. More recently, among the new amorphous materials with potential applications, there has been increasing interest in the deposition of a special form of carbon films [2]. These films have been called "diamond like" or "diamond black", and are obtained by low energy ion-beam deposition [3],

RF-plasma deposition of a hydrocarbon gas [4], ion beam sputtering [5], and ion plating techniques [6].

Carbon in its crystalline form can exist either in threefold coordination as graphite, a semimetal, or in fourfold coordination as diamond, an insulating wide band gap semiconductor. It can also exist in the amorphous state and possess intermediate properties depending on the deposition conditions. Hard "diamond-like" amorphous carbon films, with properties closer to those of diamond than to those of graphite, include extreme hardness, chemical inertness, high electrical resistivity, optical transparency in the infrared, and a wide optical gap [2].

A great number of analytical techniques have been employed recently to characterize the properties of this material. Hardness measurements as a function of deposition conditions have been investigated by Hiraki *et al.* [7]. The luminescent properties have been reported by various groups. Watanabe and Inoue [8] studied the dependence of the photoluminescence emission on the temperature of the substrate during deposition. They found that maximum luminescence corresponded to substrate temperatures in the range of  $250 \pm 50^\circ\text{C}$ . Lin and Feldman [9] interpreted the structure of the photoluminescence emission in terms of the interaction between excited pairs (electron-hole) and acoustic phonons. Raman scattering was previously utilized to study the structure of a-C:H films prepared by various techniques [10]. In these studies, crystallization into a graphitic structure by heat treatment at temperatures above  $300^\circ\text{C}$  is reported.

The existence of a two-phase mixture of threefold graphitic and fourfold diamond-like material has been suggested to explain some of these properties [10, 11]. There are, however, some authors that have interpreted their experimental data based on a single phase model [12, 13]. Thus, from available reported data, still remains some uncertainty concerning bonding and the origin of diamond-like properties in a-C:H films.

In the present work, several optical techniques have been used to characterize the structure of hydrogenated amorphous carbon films with hydrogen concentrations in a wide range. Films prepared at low RF-powers possess more hydrogen and the characteristics of polymers, *i.e.*, they are soft, transparent and the molecular units making up the solids are only slightly modified from the starting gases. Higher RF-powers produced harder and more optically dense films. In agreement with several other authors [10, 11], our results suggest: a structure consisting of islands with graphitic-like structure embedded in an amorphous carbon matrix having mainly diamond-like coordination. The volume fraction of the graphitic part can be increased by raising the RF-power density during deposition.

## 2. Sample preparation

A set of hydrogenated a-C films were obtained from several hydrocarbons as starting gases using a RF-excitation source. The films were deposited onto

room temperature crystalline silicon and quartz substrates at RF-power densities ranging from 0.4 to 3.2 Watt cm<sup>-2</sup>. The starting gases were:



The films were all roughly one micrometer thick as determined by infrared interference measurements.

### 3. Description of analysis performed

#### a) *Vicker's hardness*

The hardness of the films was determined using a commercially available hardness tester capable of applying loading forces up to 0.5 Newtons. Blank sapphire wafers with known hardness were used as the calibration reference of our hardness tester apparatus.

b) *Infrared absorption*

Absorption spectra in the infrared (IR) range from  $4000\text{ cm}^{-1}$  to  $300\text{ cm}^{-1}$ , were obtained for all the films using a Perkin-Elmer model 580 double beam spectrophotometer. The films used for this analysis were deposited on crystalline silicon and a bare silicon piece was placed in the reference beam to minimize or eliminate peaks due to the substrate. This technique gives information about the local hydrogen-carbon atomic arrangements.

c) *Hydrogen concentration*

Hydrogen quantification was accomplished using a combination of IR and nuclear reaction (NR) techniques. The NR technique utilizes a beam of  $\text{N}^{15}$  ions which bombard the film at high energy. The interaction of the  $\text{N}^{15}$  nucleus with a H atom results in the emission of a gamma ray with a specific energy. The probability for this interaction to occur is very high only for a specific  $\text{N}^{15}$  kinetic energy, thus permitting a depth profile of hydrogen concentration to be obtained. The gamma ray yield can be calibrated to give the hydrogen concentration. Unlike IR measurements, the NR technique is insensitive to the chemical bonding arrangements and so detects both the bonded and unbounded hydrogen in the film.

d) *Visible range absorption*

The absorption coefficient in the range of 1.2 to 1.6 eV was obtained by measuring the transmittance of films deposited on glass substrates. A calibrated tungsten lamp was used as the radiation source.

e) *Raman and photoluminescence*

In order to gain more insight into how the structure of these materials influence their physical properties, extensive Raman scattering (RS) and photoluminescence (PL) measurements were performed. Any finite size effect, such as microcrystallinity, amorphicity, defects, impurities, etc., results in appreciable changes in the Raman spectra. Thus, particle size in microcrystalline materials can be determined from the details of the Raman spectra [14].

The room temperature Raman measurements were carried out using an Ar ion laser as the excitation source at power densities below  $1\text{ Watt cm}^{-2}$ . To avoid local heating, the laser beam was spread out into a vertical spot focused on the carbon film by means of a cylindrical optics. The spectral analysis of the scattered light was made using a Spex II double spectrometer, and its intensity detected with a RCA photomultiplier tube.

For the PL measurements several excitation lines from He-Ne and Ar lasers were used. Both the continuous and chopped light modes were utilized with similar results. The spectral analysis of the emitted radiation was made using a Jobin Ivon double monochromator in the range of 2.6 to 1.25 eV and detected by a RCA GaAs photomultiplier tube.

#### 4. Results and discussion

##### a) *Hardness*

The hardness of the a-C:H films depends on the RF-power density during preparation as shown by the black dots in figure 1. An increase in the RF-power density up to  $\sim 1.6$  Watt  $\text{cm}^{-2}$  results in an increase in the Vicker's hardness; for higher RF-power densities the hardness levels out and remains approximately constant with variations within the uncertainty of our experimental measurements.

The reported range in the Vicker's hardness for natural diamond and natural sapphire are shown for comparison [15]. Notice that a-C:H films with hardness higher than natural sapphire and comparable to that of natural diamond can be obtained when RF-power densities above  $\sim 2.0$  Watt  $\text{cm}^{-2}$  are used. The dependence of hardness on the RF-power density may be related to plasma polymerization on the following terms: At low RF-power densities the decomposition of the gas molecules is not severe and the deposited species differ only slightly from the starting gas molecules. These films have characteristics of polymers, *i.e.*, they are soft and transparent. At high enough RF-power densities, the starting gas molecules are decomposed sufficiently so that a larger amount of atomic carbon or carbon rich species reach the substrate. This enables the formation of a larger amount of single, double and triple carbon-carbon bonds which increase the average bond strength and, consequently, the film hardness. Experimental evidence of the higher degree of carbonization for those films will be presented in coming sections.

Shown in the same figure 1 (triangles) is the optical density at 2.4 eV versus RF-power density. The increase in the optical density for higher RF-power is related to the higher degree of carbonization, as discussed in the paragraph above. More details on the absorption in the visible range will be presented in coming sections.

Due to its hardness, lubricity, resistance to wear and to corrosion, and because it can be applied to various surfaces in very thin films, a-C:H is a very attractive coating material for enhancing the durability of various industrial and consumer products.

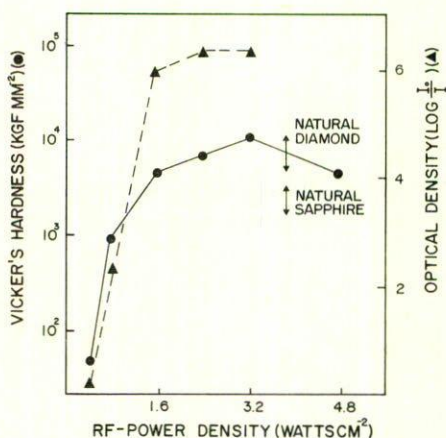


FIGURE 1. Vicker's hardness and optical density for the a-C:H films prepared at various RF-power densities.

### b) IR measurements

Infrared absorption occurs due to vibrations between unlike atoms or groups of atoms. Therefore, in a-C:H films, absorption is strongest for C-H vibrations (stretch, deformation and wag) and zero (or very weak) for C-C bond vibrations.

There are five groups of vibrations commonly observed in hydrocarbon materials [16]:

1) C-H methyl and methylene stretch groups. These are the strongest absorbers.

- CH<sub>3</sub> asymmetric stretch at 2960 cm<sup>-1</sup>.
- CH<sub>2</sub> asymmetric stretch at 2930 cm<sup>-1</sup>.
- CH<sub>3</sub> and CH<sub>2</sub> asymmetric stretch at 2860 cm<sup>-1</sup>. For a C atom having a double bond, the =CH<sub>2</sub> stretch at 3020 cm<sup>-1</sup>. For a C having a triple bond (acetylene), the ≡CH stretch appears at 3310 cm<sup>-1</sup>.

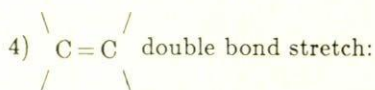
2) CH<sub>2</sub> and CH<sub>3</sub> deformation modes.

- CH<sub>3</sub> asymmetric and —CH<sub>2</sub> symmetric (scissors mode) appear at 1460 cm<sup>-1</sup>.
- CH<sub>3</sub> symmetric mode appear at 1375 cm<sup>-1</sup>.

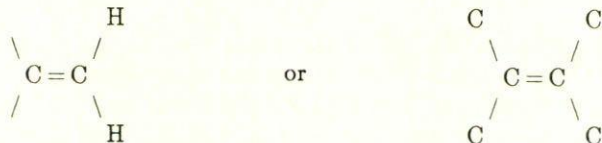
3) Olefin wag modes. These are out of plane motions of the H atoms in the following configuration:



There are fairly weak features at approximately  $975\text{ cm}^{-1}$  and  $890\text{--}910\text{ cm}^{-1}$ . The plus sign indicates that the H atoms are moving in phase, out of the molecule plane.

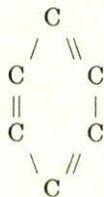


This is a symmetric vibration with no change in the dipole moment and therefore it should not appear in the IR spectrum. However, if the atoms attached to the two carbon atoms are such that the symmetry of the whole unit is not preserved, then some IR absorption can occur. For instance situations such as



can lead to IR absorption. In addition, there is an IR active mode in graphite. This is an in-plane motion of carbon atoms requiring at least two graphite planes to be active. This absorption occurs at  $1587\text{ cm}^{-1}$ .

5) Benzene modes



In a monosubstituted benzene group the C-H stretching vibrations give rise to multiple bands in the region  $3100\text{--}3000\text{ cm}^{-1}$ . The C-H out-of-plane bonding vibrations give rise to bands in the region  $1000\text{--}700\text{ cm}^{-1}$ . In these vibrations a carbon and its hydrogen move in opposite directions. Vibrations involving C-H in-plane bending are found throughout the  $1600\text{--}1000\text{ cm}^{-1}$  regions.



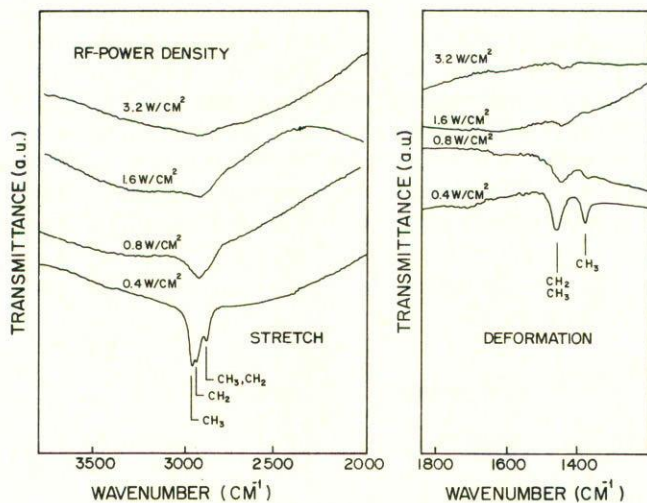


FIGURE 3. Infrared spectra of films prepared from methane gas at different RF-power densities.

Films prepared from benzene exhibit a richer IR spectrum. The modes in the 700–900  $\text{cm}^{-1}$  range involve out-of-plane ring bending and out-of-plane C-H wag modes of substituted benzenes. The modes at 1027, 1073, 1450, 1500  $\text{cm}^{-1}$  correspond to normal modes of vibration of the monosubstituted benzene ring, sometimes strongly mixed with single carbon-carbon vibrations. The absorption bands at about 1600  $\text{cm}^{-1}$  correspond to stretching vibrations of double bonded carbon in a benzene configuration. The aromatic C-H stretching vibrations give the absorption in the range of 3000–3100  $\text{cm}^{-1}$ . The presence of the methyl and methylene groups in the range of 2900–3000  $\text{cm}^{-1}$  indicate that dissociation of the benzene rings has taken place.

Figure 3 shows the IR spectra of films prepared from methane gas at different power densities. At the lowest power we observed well defined  $\text{CH}_2$  and  $\text{CH}_3$  stretch ( $\sim 3000 \text{ cm}^{-1}$ ) and deformation ( $\sim 1400 \text{ cm}^{-1}$ ) modes. At higher power densities the  $\text{CH}_2$  and  $\text{CH}_3$  peaks in the stretching and deformation modes become broader and their intensity diminishes and almost disappears at the highest RF-power density. In figure 3 the integrated absorption area can be used for a direct comparison of the hydrogen concentration, because the measurements were done in samples having approximately the same thickness and with the same aperture in the IR spectrophotometer. Note that the gradual reduction of the deformation modes is faster for the  $\text{CH}_3$  symmetric vibration indicating richer hydrogen films at lower powers.

In general, the effects on the hydrogen configuration with increasing power for the other starting gases is similar to those observed in figure 3. An overall

diminishing and broadening occurs in the absorption bands as the power increases. At the highest power density the absorption spectrum looks similar for all the films regardless of starting gas. The implication is that at high enough RF-powers the original molecules are severely broken up, and therefore the species reaching the substrate are similar in all cases, and so is the film structure.

We have also prepared films from various hydrocarbon gases diluted with argon gas at various ratios. Increasing the diluent gas has effects similar to increasing RF-power. That is, the absorption due to double bonded C-C atoms appears around 1000 and 1600  $\text{cm}^{-1}$ .

### c) Quantification of hydrogen concentration

The amount of bonded hydrogen is an important quantity to determine. Two analytical methods were used for this purpose, and at the present time only the methane films have been quantified. As mentioned above, the analysis was made using IR and nuclear reaction techniques.

Looking back at figures 2 and 3, one sees that the strongest absorption bands are the methylene stretch and deformation modes. The integrated absorption of one of these bands can be related to the number density or concentration of the bonds producing the absorption by means of the expression

$$\frac{1}{d} \int \alpha(\nu) d\nu = DA, \quad (1)$$

where  $\alpha(\nu) = \ln(I(\nu)/I_0(\nu))$ ,  $\nu$  is the frequency in  $\text{cm}^{-1}$ ,  $d$  is the film thickness,  $I(\nu)$  the measured intensity at  $\nu$ ,  $I_0(\nu)$  the incident intensity at  $\nu$ ,  $D$  the number of bonds per cubic centimeter, and  $A$  is the change in the dipole moment with respect to the motion of the bond. Assuming that  $A$  is a constant for a particular absorption mode of a particular unit, a standard sample can be measured to determine  $A$  and then  $D$  can be calculated as long as an accurate film thickness is known. Polyethylene was chosen as a standard sample because it has a molecular structure similar to our  $\text{CH}_4$  deposited films. From the integrated absorption of a stretch mode and taking  $0.92 \text{ g/cm}^3$  as the polyethylene density we have found a value for  $D = 3.96 \times 10^{22} \text{ CH}_2 \text{ bonds cm}^{-3}$ , using equation (1), we obtain  $A = 6.46 \times 10^{-19} \text{ cm/CH}_2 \text{ bond}$ . Using the same procedure, the total calculated amount of hydrogen is shown in figure 4. The error bars arise from two possible sources, the first is from the uncertainty in the decomposition of the  $\text{CH}_2$  and  $\text{CH}_3$  modes due to their proximity and the second is from the modeling of the interference patterns in order to determine  $I/I_0$  accurately.

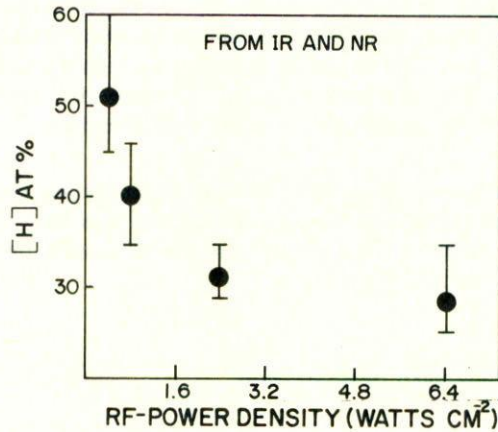


FIGURE 4. Atomic hydrogen concentration for films prepared from methane gas at different RF-power densities.

Although the hydrogen concentrations determined from nuclear reactions are in good agreement with IR measurements, we found consistently lower values with the former technique. Recent studies on the effects of ion bombardment of a-C:H films have shown that irradiation by ions provokes hydrogen out-diffusion [17]. The model suggested is that when a C-H bond is broken by the collision between the impinging ion and the target atoms, the hydrogen is free to diffuse out of the film as molecular hydrogen.

#### d) *Optical absorption*

The optical spectra provide useful information on the structure of amorphous carbon. The absorption data in many amorphous semiconductors can be divided into two regions, above and below  $\alpha \sim 10^4 \text{ cm}^{-1}$ , with  $\alpha$  being the absorption coefficient. In the upper region the electronic states involved are necessarily delocalized with a parabolic density of states at each edge. If these conditions are satisfied, the energy dependence of  $\alpha$  gives a linear dependence on the Tauc's plot, written as [18]:

$$(\alpha d E)^{1/2} = B^{1/2}(E - E_{oc}), \quad (2)$$

where  $E_{oc}$  is the optical band gap,  $d$  the sample thickness,  $E$  the photon energy and  $B$  a constant.

Figure 5 shows the Tauc's plot for samples prepared at various RF-power densities. The extrapolation to zero absorption of the linear section of these curves, at high energies, yields a value for  $E_{oc} = 1.75 \text{ eV}$  for the sample prepared at  $0.4 \text{ Watt cm}^{-2}$ . An increase in the RF-power density results in a gradual

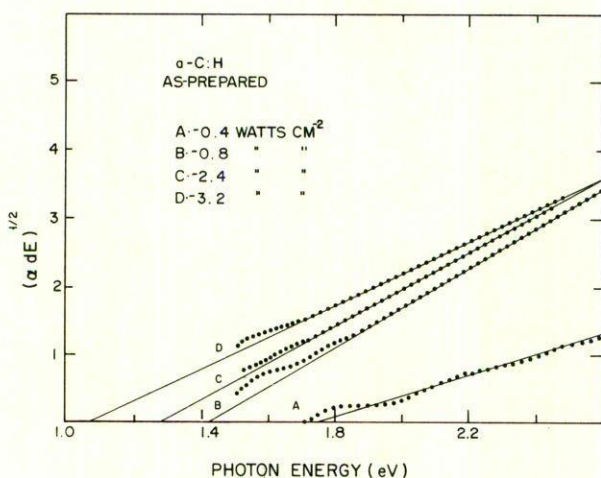


FIGURE 5. Tauc's plot for samples prepared at various RF-power densities.

decrease in  $E_{0c}$  reaching a value of 1.03 eV for samples prepared at the highest power density of 3.2 Watt  $\text{cm}^{-2}$ . The deviation from the linear behaviour in the low energy region is due to interference of the reflected light at the air-film and film-substrate interfaces.

Assuming the diphasic model for the amorphous carbon films, *i.e.*, graphitic-like regions embedded in an amorphous  $\text{sp}^3$  coordinated carbon matrix, several authors have found that the values of  $E_{0c}$  and  $B$  (Eq. 2) can be related to valuable parameters of the graphitic component [12]. The  $E_{0c}$  gives the size of the largest significant cluster and the slope,  $B$ , gives the range of cluster size. Furthermore, it has been found that the optical gap for finite clusters of fused sixfold rings follows the relation,  $E_{0c} = 5.8M^{-0.5}$  [2], where  $M$  is the number of rings. From this relation we calculated that in our materials, gaps of 1.07 and 1.75 eV need clusters with 29 benzene rings for the former and 11 benzene rings for the latter; this is equivalent to graphitic planes with lateral dimensions of 15 Å and 8 Å respectively.

In figure 6 we have plotted the variation of the  $E_{0c}$  (from Fig. 5) for samples prepared at different RF-power densities versus the hydrogen concentration (from Fig. 4). The corresponding inverse particle size,  $L^{-1}$ , is given in the right vertical scale. As can be seen, for lower hydrogen concentrations the graphite particles are larger and their size decreases as the hydrogen concentration increases. This behavior can be understood considering that at sufficiently high RF-power the starting gas molecules are broken up into their atomic constituents, and thus the lack of hydrogen in the growing film favors the formation of the graphitic structure, the allotropic form of carbon with lowest energy.

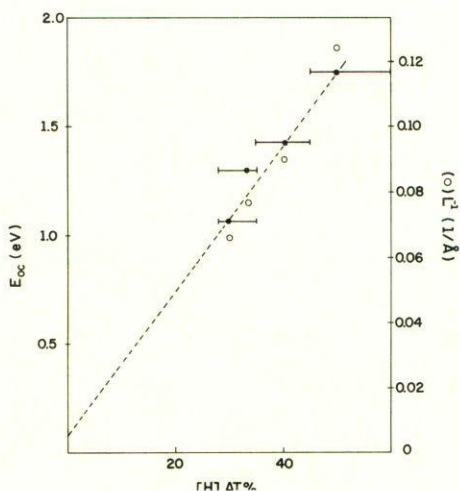


FIGURE 6. Variation of  $E_{oc}$  (from Fig. 5) vs. hydrogen concentration (from Fig. 4) for samples prepared at different RF-power densities.

It is important to notice that the extrapolation of the straight line to zero hydrogen concentration in figure 6 predicts, within the error bars, a zero energy gap, which is expected for an infinite graphite plane.

It is significant that independent particle size measurements by Raman scattering are in excellent agreement with the optical measurements. Raman measurements will be presented later in this paper.

#### e) *Photoluminescence*

In figure 7 we show the photoluminescence spectra for samples deposited at various RF-power densities. All of the spectra were taken at room temperature with the same collection aperture. The vertical scale in the figure is not the same for all curves, therefore comparison of the absolute PL intensity is not possible. Absolute values of the PL intensity are given in figure 8. Returning to figure 7, power densities of  $0.4 \text{ Watt cm}^{-2}$  result in three main features in the PL spectra, which are located at 1.9, 2.2 and 2.4 eV. When the power density is increased to  $0.8 \text{ Watt cm}^{-2}$  a red shift in the three main bands is observed. Notice that a strong anti-Stokes PL component is present in the emission spectra of these materials indicating that a multi-step process may be involved. Further increase in the RF-power density results in a new feature in the spectra. At RF-powers of  $1.6 \text{ Watt cm}^{-2}$  or higher, superimposed on the PL spectra, there appear sharper peaks located approximately at 2.2 and 2.38 eV when the  $4880 \text{ \AA}$  is used as the excitation line. Those peaks correspond to the second-order (2.2 eV) and the

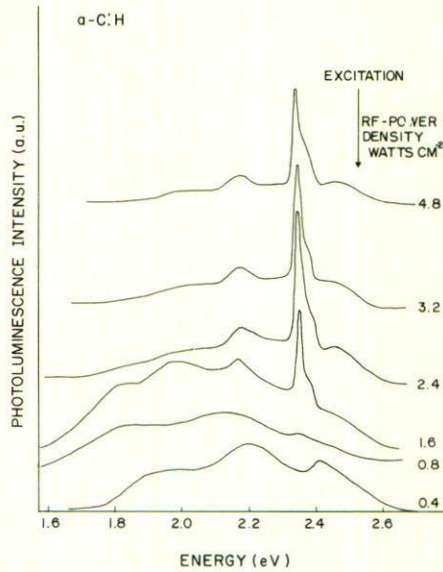


FIGURE 7. Photoluminescence spectra for samples deposited at various RF-power densities.

first-order (2.38 eV) Raman scattering of the optical phonons in a graphitic-like structure.

In figure 8 we show the integrated PL intensity per absorbed photon as calculated from figure 7. In order to take into account the increase in optical absorption as the RF-power is increased, the integrated PL intensity was normalized to the number of absorbed photons at 2.5 eV, energy of the excitation. The change in the optical density at this energy with the RF-power density is shown as an inset at the left lower corner of the figure. It can be seen that there is a rapid decrease in the PL intensity by almost two orders of magnitude when the RF-power density is increased from 0.8 to 3.2 Watt  $\text{cm}^{-2}$ . The lower emission efficiency is related to the hydrogen concentration in the films. Higher RF-power densities result in lower hydrogen concentration and therefore a larger density of nonradiative recombination centers, possibly dangling bonds.

As pointed out in section 4d, the existence of an optical gap with a width depending on RF-power density, requires the presence of  $\text{sp}^2$  sites clustered together. What was surprising, at first, was that the whole PL emission spectrum of each sample in figure 7 occurs at energies above the corresponding energy gap (Fig. 5). This apparently contradictory result can be explained in terms of the structural model of two mixed phases: graphitic-like regions connected by a fourfold coordinated amorphous carbon network.

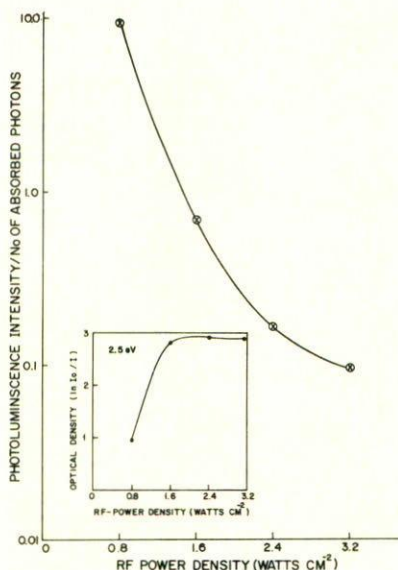


FIGURE 8. Integrated photoluminescence intensity for samples prepared at various RF-power densities. The inset shows the optical density at 2.5 eV.

We believe that the photoluminescence is originated in the diamond-like component based on the following experimental observations:

- a) Firstly, if we compare the spectra in figure 7 we see that regardless of the deposition RF-power, the broad luminescence emission is roughly located at the same energy for all samples.
- b) As can be seen in figure 9, the emission spectra depends on the excitation energy. Higher excitation energies provoke a blue shift of the whole PL spectrum. This indicates that the electronic states involved in the PL emission are localized up to energies of at least 2.9 eV and therefore that the band gap of this phase is greater than the maximum photon energy used for excitation.
- c) The photoluminescence spectra of several plastic materials having molecular units similar to those observed in our a-C:H films occur at energies in the same range as those of the a-C:H films (Fig. 10).

Although some authors have found that polycrystalline graphite shows a weak PL emission at energies similar to that of the emission in a-C:H films [19], they have concluded that the weak emission is probably occurring between energy states associated with impurities located either at grain boundaries or in the volume of the grains. In the present work, measurements in our clean amorphous

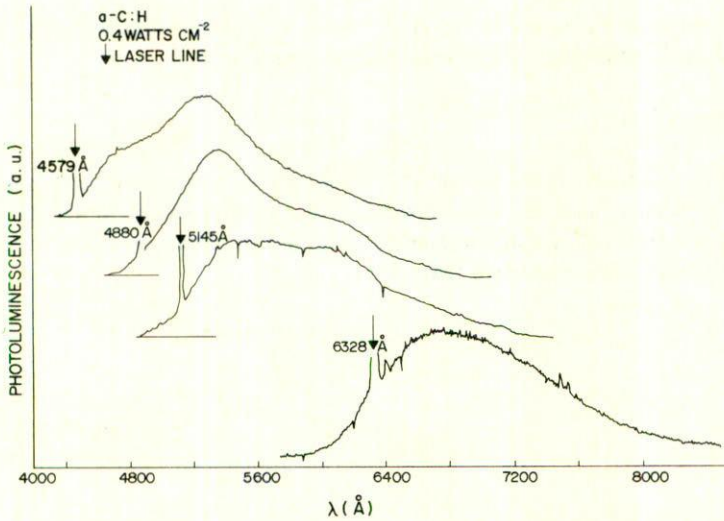


FIGURE 9. Excitation photoluminescence emission spectra for an a-C:H film prepared at 0.4 Watt  $\text{cm}^{-2}$ . The energy of the excitation corresponds to the 6328 Å of He-Ne; 4880 Å, 5145 Å and 4579 Å of  $\text{Ar}^+$ , laser lines.

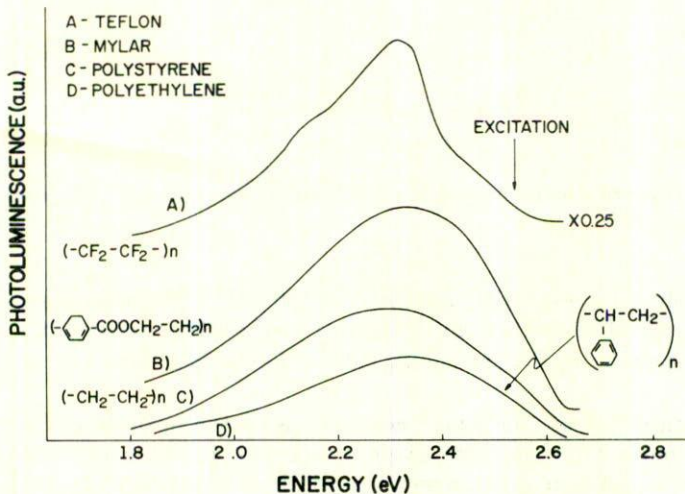


FIGURE 10. Photoluminescence spectra of several plastic materials with molecular units similar to those observed in the a-C:H films.

carbon films with and without hydrogen indicate that the PL intensity is strongly dependent on the degree of graphitization. Thus, samples produced at high RF-power densities or by annealing at elevated temperatures with a highly graphitized

structure show no measurable PL. This result is in agreement with the impurity related photoluminescence in polycrystalline graphite.

#### f) Raman scattering

To investigate in more detail the structure of the graphitic component a systematic Raman analysis was performed in all samples. In figure 11 we show details of the first-order Raman spectra obtained by slow scan runs in the a-C:H samples. The spectra show two features:

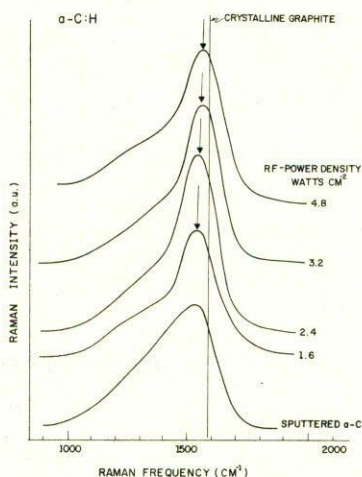


FIGURE 11. First-order Raman spectra of a-C:H films prepared at various RF-power densities.

- 1) A relatively sharp line, with a width of  $\sim 150 \text{ cm}^{-1}$ , whose frequency position in the range of  $1500\text{--}1570 \text{ cm}^{-1}$  depends on the RF-power density.
- 2) A broad shoulder at the low energy side of the sharper line.

The vertical line at  $1590 \text{ cm}^{-1}$  corresponds to the position of the only Raman active mode for a graphite single crystal [19] in the energy range shown in the figure. From our measurements a width of approximately  $15 \text{ cm}^{-1}$  was obtained for this peak. For comparison we have also included (bottom curve) the Raman spectra of a nonhydrogenated sample prepared by RF-Sputtering from a graphite target. Notice that in this curve the two features observed in the a-C:H samples are no longer distinguishable and instead a broad asymmetric line is observed. Previous studies have shown that a similar broad asymmetric Raman line is characteristic of amorphous carbon with full  $sp^2$  coordination [20]. What

is clear from figure 11 is that there is a difference between the Raman spectra of hydrogenated and unhydrogenated carbon materials. Because higher RF-power densities favor the formation of  $sp^2$ , as shown by IR measurements, one would expect some changes in the Raman spectra. If the increase in RF-power produces isolated  $sp^2$  sites one should observe an increase in the intensity of the Raman line associated with those sites but no change in the line shape. However, we see that the line narrows and approaches the frequency of the Raman peak for crystalline graphite. To our understanding, this indicates that the graphitic sites are clustered together. The structure of these graphitic-like regions can be analyzed looking into the details of their Raman spectra. The most obvious changes in the Raman spectra are its red shift and narrowing for higher RF-power, which can be accounted for in terms of two possible mechanisms:

- i) An increase in short range order of amorphous graphitic-like regions, *i.e.*, reduction in bond-angle distortion.
- ii) An increase in size of crystalline graphitic-like regions.

Let us assume that the latter mechanism is correct. Following the method proposed by Richter *et al.* [14] for microcrystalline silicon and now applied to several other microcrystalline materials, one can estimate the correlation length,  $L$ , of the graphite layers. This model is based on the relaxation of the phonon momentum conservation selection rule due to microcrystallinity. Momentum conservation in a graphite single crystal dictates a sharp peak from the zone-center optical phonons located at  $\sim 1590 \text{ cm}^{-1}$  that has been previously identified as the  $E_{2g_2}$  mode [21]. However phonon localization by crystal imperfections such as grain boundaries, results in a partial breakdown of the phonon momentum conservation selection rule. And since the phonon dispersion curve for graphite has a maximum at  $1590 \text{ cm}^{-1}$  the frequency,  $\omega$ , of the phonon when confined to a spacial region with lateral dimensions,  $L$ , is lowered depending on  $L$ . The size dependence comes from the  $\Delta qL = 1$  rule (Heisenberg's uncertainty principle), with  $\Delta q$  being the uncertainty in the phonon momentum given by  $\Delta q = L^{-1}$ . To determine the larger size from the Raman spectra, one needs to know the phonon dispersion relation  $\omega(q)$  [22]. Considering that graphitic layers in the  $100 \text{ \AA}$  range size have a  $|\Delta q|$  within one tenth of the Brillouin zone length, one can assume a linear behaviour for  $\omega(q)$ , *i.e.*  $\omega = Cq$  with  $C$  a constant. From the phonon dispersion relations for a single graphitic layer the value of  $C = 2.25 \times 10^{-6}$  has been obtained and therefore the layer size is given by  $L = 2.25 \times 10^{-6} / \Delta\omega$ , where  $\Delta\omega$  is the measured Raman shift. Typically we measured values for  $\Delta\omega$  of 15 and  $50 \text{ cm}^{-1}$  for the samples prepared at RF-power densities of 3.2 and  $1.6 \text{ Watt cm}^{-2}$  respectively.

Substituting those values into the expression for  $L$  we obtain  $L = 15 \text{ \AA}$  and  $5 \text{ \AA}$  respectively. These numbers for  $L$  must be compared with the ones obtained in section 4d using the optical absorption data. Within experimental error, it is observed that a larger cluster size is obtained from the optical data. This might be due to the fact that the  $E_{oc}$  measures the size of the largest significant cluster, whereas the Raman measurement is the superposition of various lines occurring at slightly different frequencies with a maximum intensity at a frequency characteristic of the most frequent layer size.

The excellent agreement in the crystallite size obtained with both the optical absorption and Raman techniques, lead us to conclude that the graphitic-like regions are crystalline in nature. However, PL measurements indicate the existence of a different phase with a much wider band gap, characteristic of a diamond-like coordination. The whole set of measurements reported here can be understood in terms of the following structural model: graphitic-like microcrystalline regions embedded in an amorphous diamond-like network.

It must be pointed out that to our knowledge, this is the first time that the PL emission in these materials has been satisfactorily explained by means of a diphasic structural model.

## 5. Conclusions

To summarize, we can make some general statements about what the materials are and the processes that take place during deposition. We found that in depositions at low RF-power densities, the molecular structure of the starting gas is propagated into the structure of the film. This is a weak plasma polymerization stage. The majority of the structural units are held together by cross-linking molecules in the form of methyl and methylene groups. The film characteristics are those of a typical polymer, *i.e.*, soft, transparent, highly resistive and chemically inert.

Higher deposition powers break the starting molecules to a greater extent and the species in the plasma can no longer be identified with any particular molecule. There is an increase in the density of C = C double bonds resulting in a larger visible optical absorption.

According to band structure calculations in carbon materials [2], six member rings, as in graphite, are necessary for the material to have a band gap. The width of the gap is inversely proportional to the size of the planes formed by these rings. From the optical absorption measurements, we found optical gaps which depend inversely on the degree of graphitization. However, the photoluminescence emission always occurs at energies above the measured optical band gap. These results along with Raman measurements indicate that the structure of the a-C:H films consists of a mixture of two phases: one, crystalline clusters of carbon atoms with  $sp^2$  coordination embedded in the second phase composed mainly of C-C

and C-H bonds with  $sp^3$  coordination like in amorphous diamond. The first phase being responsible for the optical band gap and the second giving rise to the photoluminescence emission.

## Acknowledgments

This work was partially supported by the Fundación R.J. Zevada of México under contract # 58/87. One of us (R.A.) thanks CONACyT-México for partial support (contract # 84/2362). We thank S.S. Chao for many helpful discussions, and Pilar Cassy and Pilar Moreno for the typing of the manuscript.

## References

1. N.F. Mott and E.A. Davis, *Electronic Processes in Non-crystalline materials*, Clarendon Press, Oxford, UK (1979).
2. J. Robertson, *Adv. in Phys.* **35** (1986) 317.
3. S. Aisenberg and R. Chabot, *J. Appl. Phys.* **42** (1971) 2953.
4. M. Ojha and L. Holland, *Thin Solid Films* **40** (1977) L31.
5. B.A. Banks and S.K. Rutledge, *J. Vac. Sci. Technol.* **21** (1982) 807.
6. C. Weissmantel, K. Bewilogua, K. Breuer, D. Dietrich, U. Ebersbach, H.J. Erler, B. Rau and G. Reisse, *Thin Solid Films* **96** (1982) 31.
7. A. Kiraki, T. Kawano, Y. Kawakami, M. Hayashi and T. Miyasato, *Solid State Comm.* **50** (1984) 713.
8. I. Watanabe and M. Inoue, *Jpn. J. Appl. Phys.* **22** (1983) L176.
9. S.H. Lin and B.J. Feldman, *Phys. Rev. Lett.* **48** (1982) 829.
10. A. Reyes Mena, J. González-Hernández and R. Asomoza, *E-MRS Meeting, Vol. XVII*, June (1987) 229.
11. R. Grigorovici, *Amorphous and Liquid Semiconductors*, J. Tauc (Ed.), Plenum, London, UK (1974) 45.
12. K. Fujii, N. Shohata, M. Mikami and M. Yonezawa, *Appl. Phys. Lett.* **47** (1985) 370.
13. D.A. Anderson, *Philos. Mag.* **35** (1977) 17.
14. H. Richter, Z.P. Wang and L. Ley, *Sol. State Comm.* **39** (1981) 625.
15. *Handbook of Chem. and Phys.*, 58th edition, CRC-Press (1978).
16. N.B. Colthup, L.H. Daly and S.E. Wiberley, *Introduction to Infrared and Raman Spectroscopy*, Academic Press, New York, USA (1975).
17. J. González-Hernández, J. Rickards, R. Asomoza, A. Reyes-Mena, S.S. Chao and D. Pawlik, *J. of Vac. Sci. and Technol. A* (May-June 1987) part II.
18. J. Tauc, R. Grigorovici and A. Vancu, *Phys. Stat. Sol.* **15** (1966) 627.
19. R. Tsu, J. González-Hernández, I. Hernández-Calderón and C.A. Luengo, *Solid State Comm.* **24** (1977) 809.
20. B.S. Elman, M.S. Dresselhaus, G. Dresselhaus, E.W. Maby and H. Mazurek, *Phys. Rev.* **B24** (1981) 1027.
21. F. Tuinstra and J.L. Koeing, *J. Chem. Phys.* **53** (1970) 1126.
22. R. Niclow, N. Wakabayashi and H.G. Smith, *Phys. Rev.* **B5** (1972) 4951.

**Resumen.** Se han preparado películas de carbono amorfo hidrogenado usando diferentes hidrocarburos como gases de crecimiento, en una cámara de acero inoxidable a ultra alto vacío y con una fuente de excitación RF a diferentes potencias. Fueron analizadas la dureza Vicker y las propiedades ópticas de las películas empleando absorción óptica, fotoluminiscencia Raman y espectroscopía infrarroja. Los cambios en la estructura debidos a diferentes densidades de potencia RF se relacionan con sus propiedades ópticas. Las mediciones Raman proveen evidencia de regiones tipo-grafito, mientras que la fotoluminiscencia indica la presencia de átomos de carbono con número de coordinación cuatro. La fracción de volumen de la fase tipo-grafito se ve incrementada con más altas densidades de potencia RF.